EG UK Computer Graphics & Visual Computing (2016)
Cagatay Turkay and Tao R. Wan (Editors)

Using semi-automatic 3D scene reconstruction to create a digital medieval charnel chapel

Wuyang Shui[1], Steve Maddock[2], Peter Heywood[2], Elizabeth Craig-Atkins[3], Jennifer Crangle[3], Dawn Hadley[3] and Rab Scott[4]

[1]College of Information Science and Technology, Beijing Normal University, China.P.R
[2]Department of Computer Science, University of Sheffield, Sheffield, UK
[3]Department of Archaeology, University of Sheffield, UK
[4]Nuclear AMRC, Sheffield, UK

Abstract

The use of a terrestrial laser scanner (TLS) has become a popular technique for the acquisition of 3D scenes in the fields of cultural heritage and archaeology. In this study, a semi-automatic reconstruction technique is presented to convert the point clouds that are produced, which often contain noise or are missing data, into a set of triangle meshes. The technique is applied to the reconstruction of a medieval charnel chapel. To reduce the computational complexity of reconstruction, the point cloud is first segmented into several components guided by the geometric structure of the scene. Landmarks are interactively marked on the point cloud and multiple cutting planes are created using the least squares method. Then, sampled point clouds for each component are meshed by ball-pivoting. In order to fill the large missing regions on the walls and ground plane, inserted triangle meshes are calculated on the basis of the convex hull of the projection points on the bounding plane. The iterative closest point (ICP) approach and local non-rigid registration methods are used to make the inserted triangle meshes and original model tightly match. Using these methods, we have reconstructed a digital model of the medieval charnel chapel, which not only serves to preserve a digital record of it, but also enables members of t he public to experience the space virtually.

Categories and Subject Descriptors (according to ACM CCS): I.3.5 [Computer graphics]: Computational Geometry and Object Modeling—Geometric algorithms, languages, and systems, I.3.8 [Computer Graphics]: Applications—

1. Introduction

Increasingly accurate virtual reconstructions are required for cultural heritage presentation and archaeology research, with terrestrial laser scanners (TLS) often used to acquire the source data [LNCV10]. Such scanners produce substantial amounts of data in the form of point clouds, with subsequent surface reconstruction approaches focussing on producing a digital model that is detailed and/or is suitable for virtual roaming [BTS*14, HSR13]. Our work is focussed on creating a digital model of the medieval charnel chapel at Rothwell, Northamptonshire, UK (see Figure 1).

As one of only two medieval charnel chapels in England where human remains survive in situ, Rothwell presents a rare archaeological resource for the investigation of charnelling – a funerary practice in which skeletal material is collected and stored above ground. The charnel chapel at Rothwell contains disarticulated remains that were placed in the room from its construction in the 13th century until it was abandoned, probably during the mid-16th century. The majority of the bones are now stored in two stacks in the centre of the room, however a number of crania are also located on shelves that line the north and south walls. There is very limited space between the stacks, walls and shelves: for example, the space between the shelves and the stacks is about 1m and there is only 0.5m between the eastern stack and the east wall. This makes data acquisition difficult.

Figure 1: *The medieval charnel chapel.*

We used a TLS (Leica ScanStation P20) to record the Rothwell charnel chapel data. The limited space in the charnel chapel made positioning the scanner difficult. There was a problem with

DOI: 10.2312/cgvc.20161301

occlusion due to the complex geometry, and we were also operating at the limits of accuracy for the Leica, due to the proximity of the measured objects to the scanner. Consequently, the point clouds that were produced were noisy and had missing regions, e.g. holes. Automatic reconstruction was not possible. Thus, we have used a semi-automatic approach to producing a 3D mesh from this data, which can then be used for virtual roaming of the site. This paper will present the approach we have used for the requirements of this specific application. We demonstrate that splitting the complete point cloud into multiple pieces, based on geometry, produces better results than dealing with the point cloud as a whole.

Section 2 will present related work. Section 3 will describe the stages in the 3D reconstruction pipeline we have used. Section 4 will present results and Section 5 will give conclusions

2. Related Work

In converting point clouds to high quality digital models for visual cultural heritage (see [RGRG09, VBS09]), we can consider three stages: registration of multi-view TLS data, surface reconstruction and hole filling.

When using a TLS to capture a scene, because of the limited scope of view of the laser scanner and, typically, the complexity of the data, multiple scans from different positions must be taken. These scans must then be registered. Salvi et al provide a review of registration approaches for range images [SMFF07] and Tam et al consider registration from the perspective of data fitting, including rigid and non-rigid registration [TCL*13]. Depending on the number of images, algorithms can be classified as pairwise registration and multi-view registration. Iterative closest point (ICP) is the most popular pairwise approach when an initial estimate of the relative pose is known [BM92]. Rusinkiewicz et al enumerated the variants of improved ICP algorithms and evaluated the convergence rates [RL01]. To overcome the registration error accumulation of ICP based approaches, multi-view registration was proposed to align all the range images [Pul99]. More recently, hierarchical optimization was proposed by simultaneously considering transformation and registration errors [TF15].

After registering a single point cloud, the next stage is surface reconstruction. Since the point cloud is often of the order of tens of millions of points, it is sampled [PLK*13], often uniformly, for example using Poisson-disk sampling [CCS12], to accelerate subsequent data processing. Given the down-sampled point cloud, a triangle mesh is then constructed. Implicit surface reconstructions are a popular approach to generate triangle meshes by the signed-distance function construction, iso-surface extraction and explicit representation [CBC*01]. Global or local interpolation functions are used to fit the surface approximately. Alternatives are the explicit meshing approach of the ball pivoting algorithm (BPA) or Delaunay triangulation.

Once a mesh is produced, the final stage is hole filling. These may occur in the data at different sizes for different reasons, e.g. as a result of occlusion or low reflectance when using the TLS. Many previous studies have reported hole filling algorithms for small or regular holes by extracting the boundary of the hole and interpolating the missing data according to neighbourhood [WO07]. For large holes, a geometric prior is a potentially effective approach to compute the inserted data by extracting self-similar structure [SR15] or symmetrical structure [LYW*11] from the original models or online depth databases. Filling large holes remains a challenge.

3. Semi-automatic reconstruction

The pipeline that we use for producing a 3D model of the charnel chapel from TLS data is shown in Figure 2. Section 3.1 will focus on data acquisition and pre-processing. Section 3.2 will describe how we reduce the complexity of the reconstruction process, as well as improve the final results, by interactively segmenting the complete point cloud into various regions. Section 3.3 will cover surface reconstruction and Section 3.4 the hole filling stage.

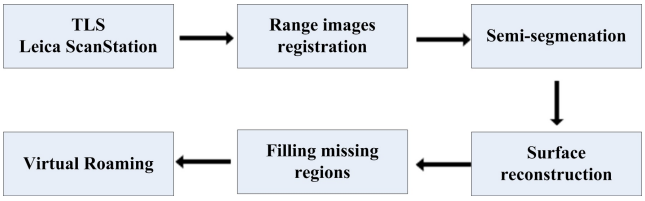

Figure 2: *The 3D reconstruction pipeline.*

3.1. Data acquisition and pre-processing

To acquire the scan data, we used a Leica ScanStation P20 (Figure 3a), a high-performance, time-of-flight (TOF) TLS, with a 360 degree horizontal / 270 degree vertical field of view, and a precision up to 3mm at 50m. 17 range images were taken in the charnel chapel (Figures 3b and 3c). Autodesk Recap 360 was used to register the 17 .pts files that were generated, producing the complete point cloud shown in Figure 3d.

3.2. Semi-automatic segmentation

The point cloud for the charnel chapel has a complex geometrical structure (which includes shelves of crania and other piles of bones in the room) and large missing regions (e.g. between the walls and shelves) due to the difficulty in positioning the TLS in the space and subsequent occlusions. The TLS used also has a minimum range of use, which was an issue in the cramped space of the charnel chapel, and contributed to some of the data inaccuracies. This makes the reconstruction process challenging since there is no one technique applicable to each of the areas, e.g. complex stacks of bones and curved roof area. To address this problem, the complete point cloud was semi-automatically segmented. The more regular areas of the entrance, the roof, the ground and the top regions of walls (above the shelves) were segmented out from the boxes of stacked bones and the wall shelves, each of which had large missing regions. This resulted in five walls and shelves, two boxes of stacked bones, the ground, the entrance and the roof. Three steps were used: point cloud pose adjustment, multiple cutting planes for coarse segmentation, and manual segmentation for regular shapes.

Principal component analysis (PCA) was used to align the point

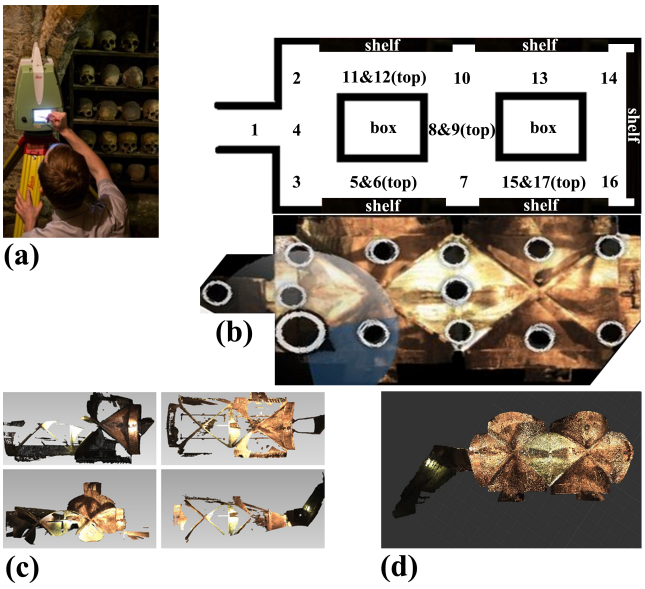

Figure 3: *The data capture process: (a) using the TLS; (b) 17 capture locations; (c) example range images from four locations; (d) the complete point cloud.*

cloud in a coordinate frame [LYZ06], with the eigenvector corresponding to the largest eigenvalue representing the x axis. Figure 4 shows the transformed point cloud and the corresponding bounding box after PCA.

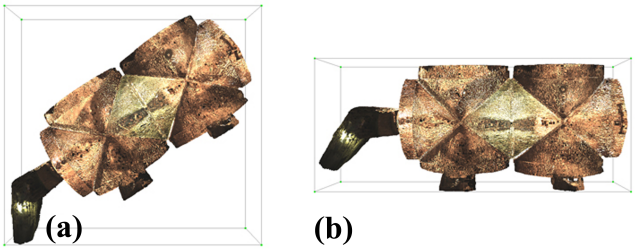

Figure 4: *Point cloud pose adjustment using PCA: (a) original point cloud; (b) transformed point cloud.*

There are approximately 60 million points in the charnel chapel point cloud, which makes selecting a region of interest (ROI) challenging. Although interactive tools such as polygon-based selection, cylinder-based selection and a lasso can be used, the overlapping spatial relationships between different objects leads to incorrect data selection. Figure 5 shows an example of point cloud region selection using the open source software Meshlab [CCC*08]. Here the rectangle extends through the point cloud. To address this problem, semi-automatic segmentation is used, which combines coarse segmentation using multiple cutting planes and manual segmentation.

A limited number of landmarks (at least three) are interactively marked on the point cloud and the least squares method (LS) is used to compute the plane equation so that a ROI can be coarsely

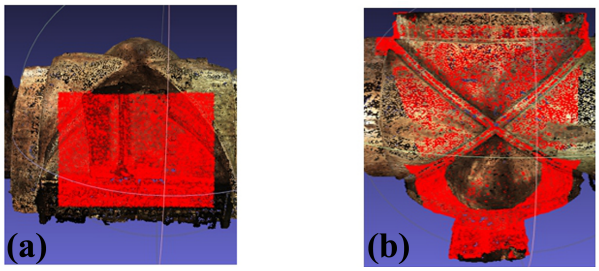

Figure 5: *The point cloud selection problem: (a) rectangle-based selection; (b) selection extended through the point cloud.*

identified. Given a set of landmarks $Q = \{q_1, q_2, ..., q_m\}, q_i = (x_i, y_i, z_i) \in \Re^3$, the plane equation is defined as $z = a_0x + a_1y + a_2$ where the coefficients (a_0, a_1, a_2) of the plane equation can be computed by optimizing the equation $S = min \sum_{i=1}^{m} \|a_0x_i + a_1y_1 + a_2 - z_i\|^2$.

Figure 6 shows an example of a shelf and wall segmentation using four cutting planes (yellow, cyan and blue planes, and the ground), each of which is determined by five landmarks. However, the stacked crania located at the bottom corner of the shelf are not accurately segmented. To address this problem, a new cutting plane can be produced along the normal vector of the cyan cutting plane, so that more of the ROI can be selected (Figures 7a and 7b). As the top regions of the shelf and wall segmentation are regular geometric shapes, which can more easily be reconstructed, they are manually removed (Figure 7c) and integrated with the roof.

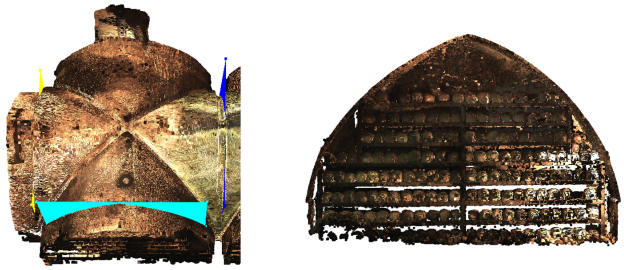

Figure 6: *The shelf and wall segmentation.*

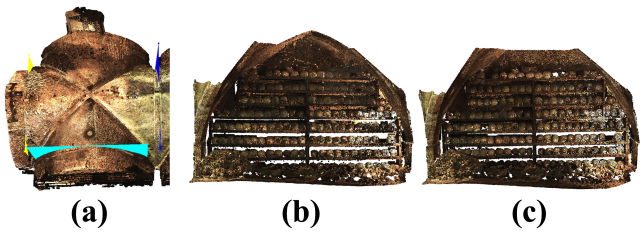

Figure 7: *(a) Multiple cutting planes; (b) accurate segmentation; (c) top region deleted.*

3.3. Surface reconstruction

To down sample from the original point cloud, both uniform and Poisson-disk sampling are used. For uniform sampling, a voxel grid is created over the input point cloud and the centroid of the point cloud set in each voxel is used as the representative point using Point cloud library [AMT*12]. Poisson-disk sampling is an effective sampling algorithm, with blue-noise properties, to generate a uniform random point set [CCS12]. Poisson-disk sampling should satisfy three properties: the distance between any two disk centres should be larger than the sampling radius; the union of the disks should cover the entire sampling domain; each point in the domain has a probability that is proportional to the sizing at this point to receive a sampling point [GYJZ15].

In this study, down sampling includes two steps. First, uniform sampling is used on the regular shapes, such as the entrance, the roof and the ground. Then, Poisson-disk sampling is used on the more complex components, including five shelf and wall pairs with crania on the shelves, and two boxes containing piles of bones.

The BPA algorithm is an effective explicit meshing method to compute a triangle mesh from a point cloud, where a ball with a given radius pivots around an active edge until touching another point [BMR*99]. The radius of the BPA affects the result of surface reconstruction. In this study, we utilize the BPA algorithm to construct triangle meshes for the sampled point clouds of each component and the radius is defined relative to the average distance (r) between neighbour points. Figure 8 shows an example of the roof and entrance reconstructed using the BPA algorithm. The radius of the top figure and bottom figure are, respectively, 10r and 25r. A larger radius is used for the small holes in the entrance and the large missing regions in the top region of the right wall. The results show that using the appropriate radius can produce high quality triangle meshes.

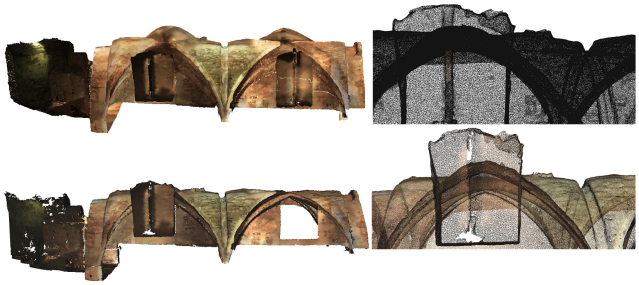

Figure 8: *Roof and entrance reconstruction using BPA algorithm.*

3.4. Missing regions filling

The most complex areas in the charnel chapel point cloud are the shelves of crania and the boxes of stacked bones. Because of occlusion to the TLS, most large missing regions are in these areas, on the walls behind the shelves and on the ground below the boxes of stacked bones. These missing regions mar the visualisation. Our analysis of the geometry suggests that planar shapes and curved surfaces are the main types of missing regions (Figures 9 and 10). The procedure for completion of large missing regions has two steps: accurate calculation of the inserted triangle meshes and surface matching.

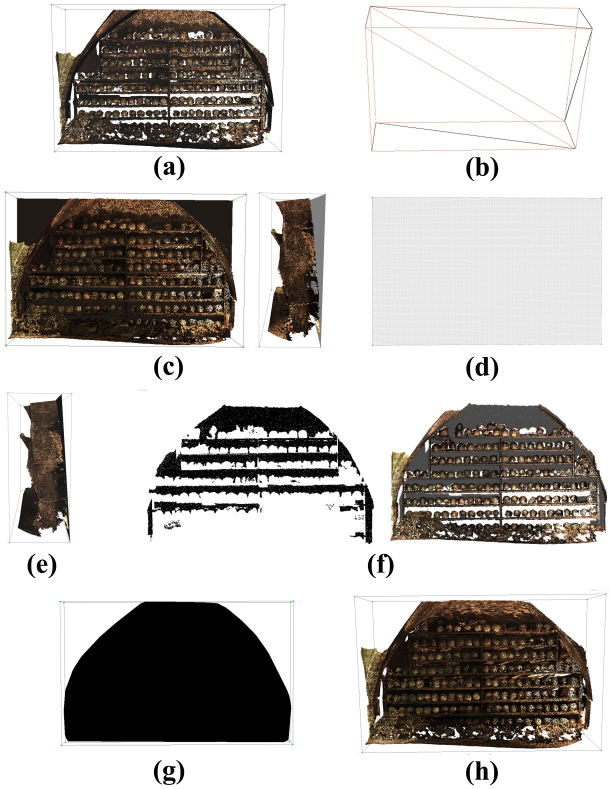

Figure 9: *Planar-shape missing regions completion. (a) The planar-shape missing region on the wall. (b) Bounding box – each of the planes consists of two triangle meshes. (c) The choice of bounding plane for calculation of inserted triangle meshes. (d) The selected plane subdivision. (e) The rigid ICP result between the bounding plane and missing region. (f) Left figure shows the projection of the shelf and wall on the bounding plane and right figure shows the comparison of projection points and original points. (g) Convex hull of projection points. (h) Final result after calculating the colour of each point on the inserted triangle meshes.*

A plane consisting of two triangles is subdivided to create a dense triangle mesh. Subsequently the ICP algorithm is used to register this bounding plane and the large missing region. Representing this bounding plane as a dense triangle mesh improves registration accuracy with the missing regions. To accurately identify the boundary of an inserted triangle mesh, the point cloud of the corresponding incomplete component is projected onto the bounding plane, using those points that are smaller than a threshold value. Finally, the convex hull is calculated to generate the inserted triangle mesh [BDH96] and the colour of each point on the inserted triangle mesh is obtained according to the nearby points on the incomplete component.

In comparison to planar-shape missing regions, it is difficult to automate the completion of missing regions of the curved surfaces.

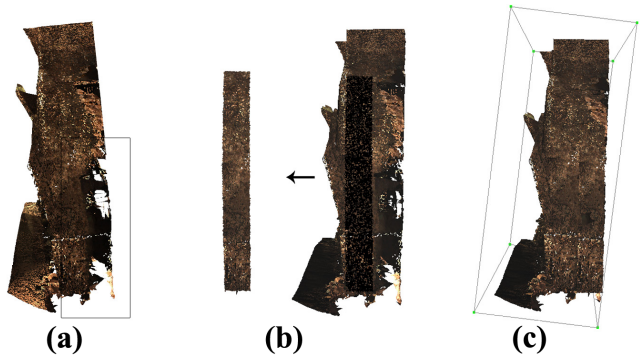

Figure 10: *Curved surface missing regions completion: (a) missing regions; (b) inserted triangle meshes after interactive selection; (c) missing regions completion.*

We interactively mark the inserted triangle meshes based on the neighbourhood of the missing regions and then these triangle meshes are interactively registered to the boundary of the holes. This effectively completes the curved surface missing regions, but at the expense of more user interaction.

Although rigid ICP is carried out to transform the inserted triangle meshes and make two models match as tightly as possible, gaps remain between the inserted triangle meshes and the original models. To solve this, we use local non-rigid registration to deform the inserted triangle meshes to the original models. A compact support radial basis function (CSRBF) is used on the inserted triangle meshes to make the inserted triangle meshes and original models tightly match. First, we find the closest point of the original model as the corresponding point for each point of an inserted triangle mesh, where a k-d tree is used to improve the speed of the searching. Then, we sort the pairs of these corresponding points according to their distances. The accuracy of corresponding pairs directly affects the result of CSRBF deformation, where some outliers should be removed according to distance, i.e. the correspondence will be rejected when the distance between corresponding points is larger than a threshold. Fig. 11 shows an example of planar-shape missing region completion after non-rigid registration.

4. Results

The charnel chapel point cloud consists of approximately 60 million points. A total of 40 landmarks and eight cutting planes have been marked on the original data, where each set of five landmarks is used to generate a plane equation for segmentation (Figure 12). Using these cutting planes and interactive selection tools, the complete point cloud has been segmented to five wall-and-shelf pairs, two boxes, the ground, the entrance and the roof. To down-sample the point clouds, uniform sampling and Poisson-disk sampling algorithms are conducted for each component, with the details shown in Table 1.

Figure 13 shows the surface reconstruction for each component from the respective sampled point clouds using the BPA algorithm.

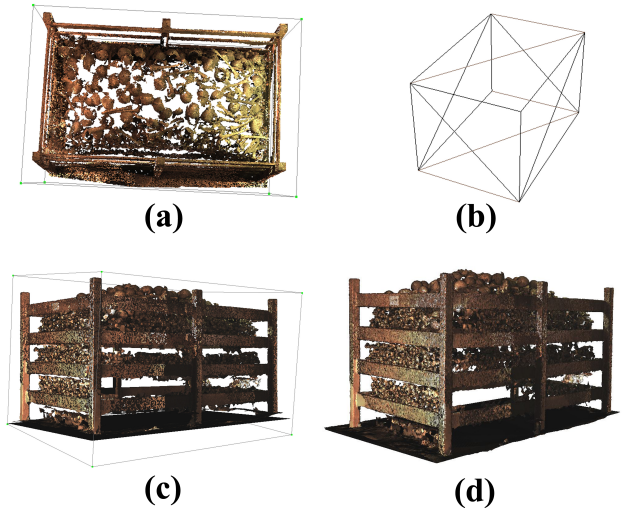

Figure 11: *Completion of missing regions using non-rigid registration: (a) missing regions; (b) bounding box; (c) interactive selection with inserted triangle meshes registered using ICP; (d) missing regions completion after CSRBF registration.*

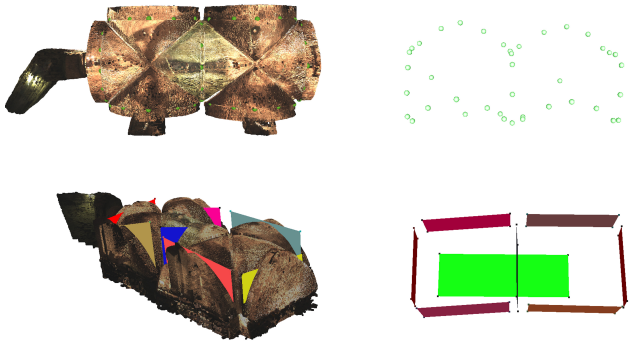

Figure 12: *Landmarks and corresponding cutting planes.*

Table 1 lists the number triangles in each mesh. Figure 14 shows the complete digital charnel chapel model after missing regions are filled. This can be compared with Figure 1.

Poisson reconstruction is the classic implicit surface reconstruction approach from oriented point clouds, with the normals affecting the reconstruction result [KBH06]. To evaluate this, we compared Poisson reconstruction with the BPA algorithm for reconstruction of the complete charnel chapel and for shelf-wall-3. Since the colour of the resulting digital model may affect the visual evaluation of reconstruction, we compare the results without colour. Fig. 15 shows the complete charnel chapel reconstruction from the sampled point cloud, where uniform sampling is carried out and a total of 0.49 million points are obtained. The BPA reconstruction produces a digital model with more details for the crania, but some holes are generated for the walls. In contrast, Poisson reconstruction produces a smooth digital model with few holes, but the detail has disappeared, and even the geometric

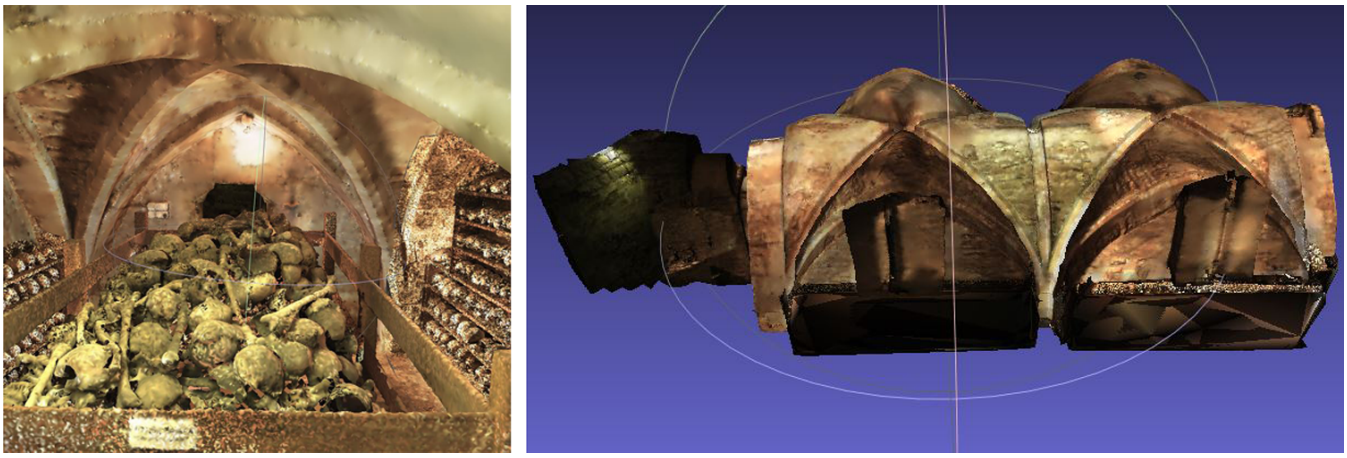

Figure 14: *Surface reconstruction for the charnel chapel (inside and outside display using Meshlab).*

Index	Original data (millions of points)	Sampling method	Sampled Points (millions)	Triangles in the mesh (millions)
roof and entrance	38.63	uniform	0.73	1.45
ground	0.12	Uniform	0.009	0.17
box-1	4.04	Poisson-disk	0.398	0.89
shelf-wall-1	2.16	Poisson-disk	0.21	0.38
shelf-wall-2	4.41	Poisson-disk	0.44	0.796
box-2	3.57	Poisson-disk	0.358	0.604
shelf-wall-3	3.91	Poisson-disk	0.388	0.685
shelf-wall-4	1.83	Poisson-disk	0.171	0.308
shelf-wall-5	1.33	Poisson-disk	0.129	0.231
Total	60.0		2.833	5.514

Table 1: *Point clouds sampling and reconstruction.*

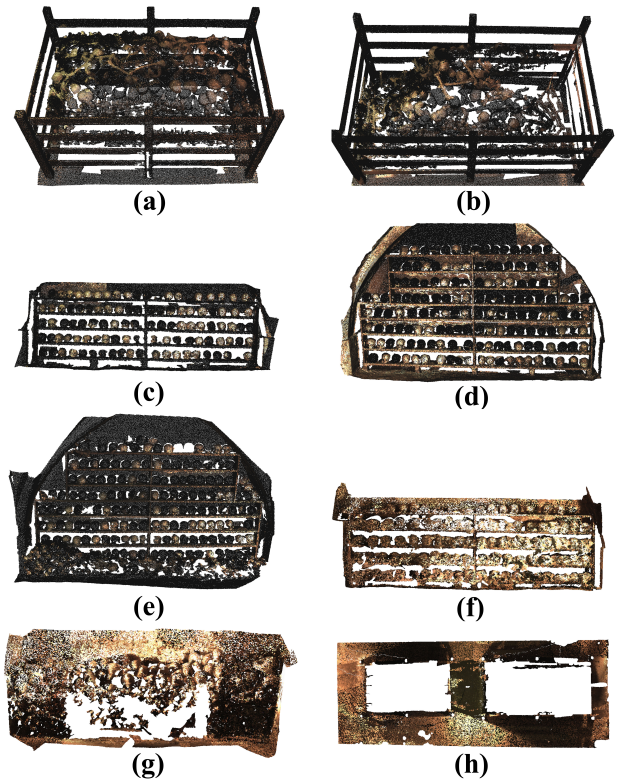

Figure 13: *Surface reconstruction for each component: (a) box-1; (b) box-2; (c) shelf-wall-1; (d) shelf-wall-2; (e) shelf-wall-3; (f) shelf-wall-4; (g) shelf-wall-5; (h) ground.*

topology on the boxes has mistakes. Figure 16 shows the results for shelf-wall-3 reconstruction using BPA and Poisson reconstruction. In comparison to Poisson reconstruction, more crania have been produced using BPA reconstruction, but large missing regions exist on the lower corner of the walls.

5. Conclusions

We have demonstrated a framework that can be used to produce a digital model from a TLS point cloud. The particular reconstruction to which we have applied this is the production of a digital model of the charnel chapel at Rothwell. We have presented a semi-automatic approach to address the challenge of dealing with large point clouds and producing a simplified mesh, suitable for virtual roaming.

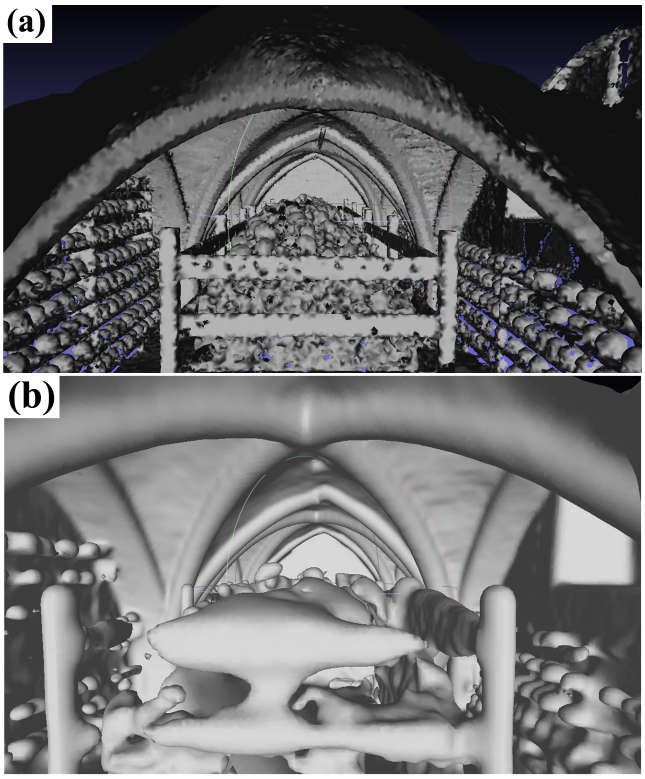

Figure 15: *A comparison between (a) BPA reconstruction and (b) Poisson reconstruction, using the complete sampled charnel chapel point cloud.*

One of the main approaches we have used is to segment the full data set into separate components based on the geometry of the scene. Multiple interactive cutting planes are employed to help a user quickly select ROIs from point clouds. Based on the use of bounding planes, a semi-automatic large missing regions completion algorithm is proposed. ICP and CSRBF are deployed to tightly match the inserted triangle meshes and the original model.

It is still a challenge to produce high quality triangle meshes with associated vertex colours, especially in user inserted regions, from TSL point clouds. This is particularly noticeable for the stacks of bones in our application. In addition, further work needs to be done to investigate approaches that can automatically complete the missing regions produced when acquiring complex geometry such as the shelves of crania in our model.

The model as it stands serves as a record of the site. In its current form it is not accurate enough to be used for detailed archaeological investigation – we plan to rescan the bones using a portable hand-held scanner. For public use, we would like to deploy the model on the Rothwell Charnel Chapel project website (http://www.rothwellcharnelchapel.group.shef.ac.uk/). For this, we are currently working on simplifying the model further and making use of texture mapping approaches to reduce the memory footprint.

Acknowledgements

The authors wish to thank the Nuclear AMRC for the loan of the Leica ScanStation P20 for the data capture stage, and Adam Wiles and Tom Hodgson, metrology engineers at the Nuclear AMRC, who worked on the data capture stage.

References

[AMT*12] ALDOMA A., MARTON Z.-C., TOMBARI F., WOHLKINGER W., POTTHAST C., ZEISL B., RUSU R. B., GEDIKLI S., VINCZE M.: Point cloud library. *IEEE Robotics & Automation Magazine 1070*, 9932/12 (2012). 4

[BDH96] BARBER C. B., DOBKIN D. P., HUHDANPAA H.: The quickhull algorithm for convex hulls. *ACM Transactions on Mathematical Software (TOMS) 22*, 4 (1996), 469–483. 4

[BM92] BESL P. J., MCKAY N. D.: Method for registration of 3-d shapes. In *Proc. SPIE* (1992), vol. 1611, pp. 586–606. 2

[BMR*99] BERNARDINI F., MITTLEMAN J., RUSHMEIER H., SILVA C., TAUBIN G.: The ball-pivoting algorithm for surface reconstruction. *IEEE transactions on visualization and computer graphics 5*, 4 (1999), 349–359. 4

[BTS*14] BERGER M., TAGLIASACCHI A., SEVERSKY L., ALLIEZ P., LEVINE J., SHARF A., SILVA C.: State of the Art in Surface Reconstruction from Point Clouds. In *Eurographics 2014 - State of the Art Reports* (Strasbourg, France, 2014), vol. 1 of *EUROGRAPHICS star report*, pp. 161–185. 1

[CBC*01] CARR J. C., BEATSON R. K., CHERRIE J. B., MITCHELL T. J., FRIGHT W. R., MCCALLUM B. C., EVANS T. R.: Reconstruction and representation of 3d objects with radial basis functions. In *Proceedings of the 28th annual conference on Computer graphics and interactive techniques* (2001), ACM, pp. 67–76. 2

[CCC*08] CIGNONI P., CALLIERI M., CORSINI M., DELLEPIANE M., GANOVELLI F., RANZUGLIA G.: Meshlab: an open-source mesh processing tool. In *Eurographics Italian Chapter Conference* (2008), vol. 2008, pp. 129–136. 3

[CCS12] CORSINI M., CIGNONI P., SCOPIGNO R.: Efficient and flexible sampling with blue noise properties of triangular meshes. *IEEE Transactions on Visualization and Computer Graphics 18*, 6 (2012), 914–924. 2, 4

[GYJZ15] GUO J., YAN D.-M., JIA X., ZHANG X.: Efficient maximal poisson-disk sampling and remeshing on surfaces. *Computers & Graphics 46* (2015), 72–79. 4

[HSR13] HINZEN K.-G., SCHREIBER S., ROSELLEN S.: A high resolution laser scanning model of the roman theater in pinara, turkey–comparison to previous measurements and search for the causes of damage. *Journal of Cultural Heritage 14*, 5 (2013), 424–430. 1

[KBH06] KAZHDAN M., BOLITHO M., HOPPE H.: Poisson surface reconstruction. In *Proceedings of the fourth Eurographics symposium on Geometry processing* (2006), vol. 7. 5

[LNCV10] LERMA J. L., NAVARRO S., CABRELLES M., VILLAVERDE V.: Terrestrial laser scanning and close range photogrammetry for 3d archaeological documentation: the upper palaeolithic cave of parpalló as a case study. *Journal of Archaeological Science 37*, 3 (2010), 499–507. 1

[LYW*11] LI X., YIN Z., WEI L., WAN S., YU W., LI M.: Symmetry and template guided completion of damaged skulls. *Computers & Graphics 35*, 4 (2011), 885–893. 2

[LYZ06] LIU H., YAN J., ZHANG D.: What is wrong with mesh pca in coordinate direction normalization. *Pattern recognition 39*, 11 (2006), 2244–2247. 3

[PLK*13] PUTTONEN E., LEHTOMÄKI M., KAARTINEN H., ZHU L., KUKKO A., JAAKKOLA A.: Improved sampling for terrestrial and mobile laser scanner point cloud data. *Remote Sensing 5*, 4 (2013), 1754–1773. 2

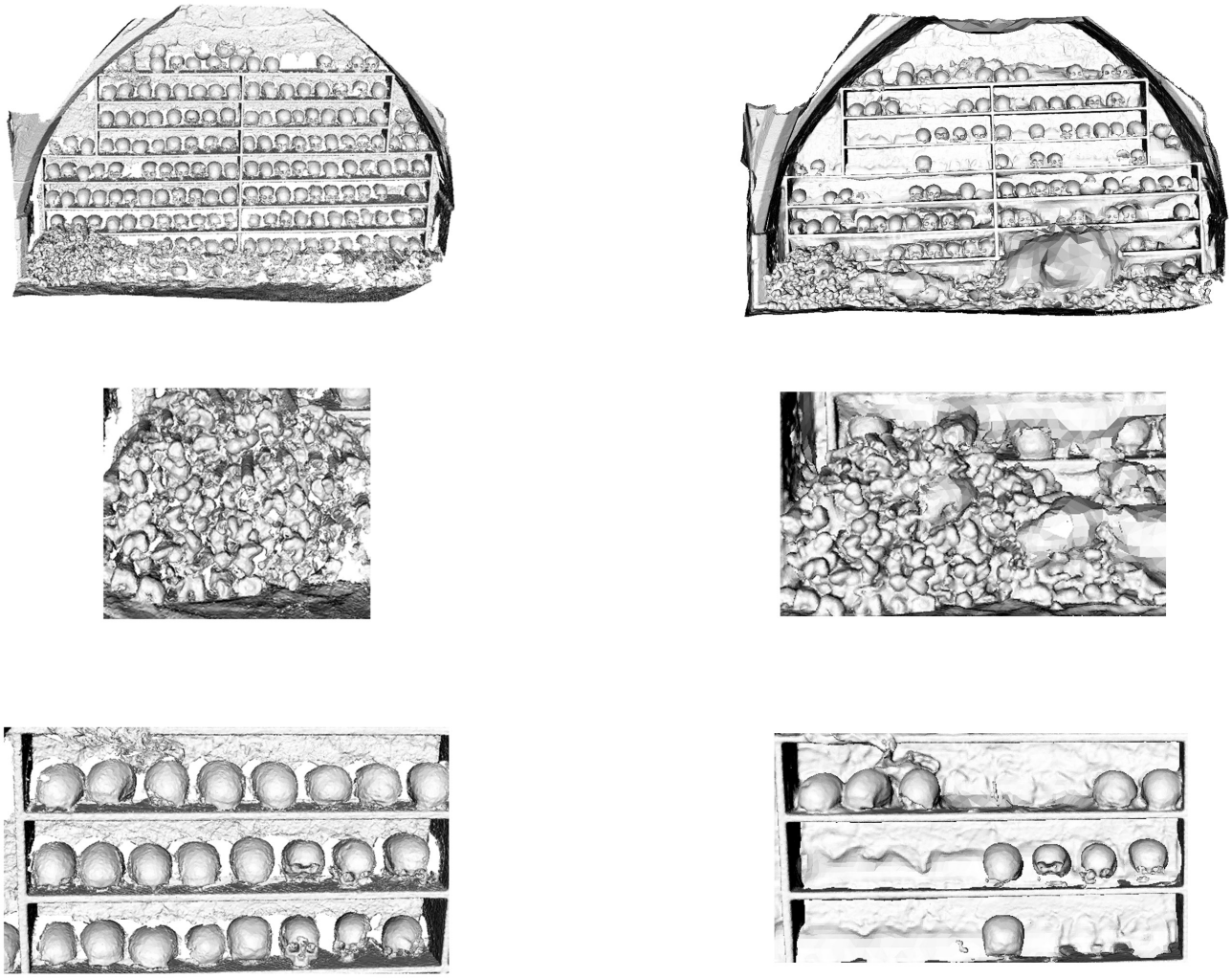

Figure 16: *A comparison between BPA and Poisson reconstruction using a shelf-wall point cloud. Left column is BPA results and right column is Poisson reconstruction results.*

[Pul99] PULLI K.: Multiview registration for large data sets. In *3-D Digital Imaging and Modeling, 1999. Proceedings. Second International Conference on* (1999), IEEE, pp. 160–168. 2

[RGRG09] REMONDINO F., GIRARDI S., RIZZI A., GONZO L.: 3d modeling of complex and detailed cultural heritage using multi-resolution data. *J. Comput. Cult. Herit. 2*, 1 (July 2009), 2:1–2:20. 2

[RL01] RUSINKIEWICZ S., LEVOY M.: Efficient variants of the icp algorithm. In *3-D Digital Imaging and Modeling* (2001), IEEE, pp. 145–152. 2

[SMFF07] SALVI J., MATABOSCH C., FOFI D., FOREST J.: A review of recent range image registration methods with accuracy evaluation. *Image Vision Comput. 25*, 5 (May 2007), 578–596. 2

[SR15] SAHAY P., RAJAGOPALAN A.: Geometric inpainting of 3d structures. In *Proceedings of the IEEE Conference on Computer Vision and Pattern Recognition Workshops* (2015), pp. 1–7. 2

[TCL*13] TAM G. K., CHENG Z.-Q., LAI Y.-K., LANGBEIN F. C., LIU Y., MARSHALL D., MARTIN R. R., SUN X.-F., ROSIN P. L.: Registration of 3d point clouds and meshes: a survey from rigid to nonrigid. *IEEE transactions on visualization and computer graphics 19*, 7 (2013), 1199–1217. 2

[TF15] TANG Y., FENG J.: Hierarchical multiview rigid registration. In *Computer Graphics Forum* (2015), vol. 34, Wiley Online Library, pp. 77–87. 2

[VBS09] VRUBEL A., BELLON O. R. P., SILVA L.: A 3d reconstruction pipeline for digital preservation. In *Computer Vision and Pattern Recognition, 2009. CVPR 2009. IEEE Conference on* (June 2009), pp. 2687–2694. 2

[WO07] WANG J., OLIVEIRA M. M.: Filling holes on locally smooth surfaces reconstructed from point clouds. *Image and Vision Computing 25*, 1 (2007), 103–113. 2